Journal of Marine Systems 98–99 (2012) 9–17

Contents lists available at SciVerse ScienceDirect

Journal of Marine Systems

journal homepage: www.elsevier.com/locate/jmarsys

Spatial and temporal variability of tidal flow in the Strait of Gibraltar

A. Sánchez-Román *, J. García-Lafuente, J. Delgado, J.C. Sánchez-Garrido, C. Naranjo

Physical Oceanography Group, CEI-MAR, University of Malaga, Campus Teatinos, 29071 Malaga, Spain

ARTICLE INFO

Article history:
Received 14 January 2011
Received in revised form 8 February 2012
Accepted 19 February 2012
Available online 7 March 2012

Keywords:
Strait of Gibraltar
Tidal currents
Seasonality
Exchange flows
Tidal transport

ABSTRACT

Recent observations collected at different places in the Strait of Gibraltar are used to investigate the temporal and spatial variability of tidal currents in this region. The analysis of a five-year long time series of velocity observations at the Espartel sill (western end of the strait) shows that harmonic constants fluctuate seasonally exhibiting smaller amplitude in winter. This fact, along with an increased subinertial flow during the winter induces a marked decrease in the relative importance of the tide to the total flow compared to the summer. New computations of tidal transport at the key sections of Espartel and Camarinal, together with historical information reported for the Eastern Exit of the strait, have been analyzed jointly to highlight the internal along-strait divergence of the tidal transport in each layer and the transfer of the tidal signal from one layer to the other. This study covers the whole length of the strait, thus extending previous results reported for the central-eastern strait. Most of the topographically forced divergence is accounted for by large vertical displacements of the interface, although velocity observations collected on the continental shelf of the northern strait suggest that coastal recirculation plays some role in the volume conservation at tidal frequencies.

1. Introduction

The Strait of Gibraltar connects the Mediterranean Sea and the Atlantic Ocean through a rather complicated system of sills and narrows. It has a length of nearly 60 km and a mean width of 20 km. The shallowest depth, less than 300 m, is found in the main sill of Camarinal (CS) and its minimum width of around 14 km coincides with the contraction of Tarifa narrows (see Fig. 1). The excess of evaporation over precipitation and river run-off, together with the conservation of mass and salt in the Mediterranean basin drive the two-layer baroclinic exchange in the Strait of Gibraltar. This exchange has been traditionally described as an inverse estuarine circulation (Stommel and Farmer, 1953) with an upper flow Q_1 of 0.81 ± 0.06 Sv ($1\ \mathrm{Sv} = 10^6\ \mathrm{m^3\ s^{-1}}$) of fresh ($S_A \approx 36.2$) and warm Atlantic water spreading into the Mediterranean basin (Soto-Navarro et al., 2010), and a westward flow Q_2 of relatively cold and salty ($S_M \approx 38.4$) Mediterranean water. The mean flow through the Strait of Gibraltar is modified by various processes at different time scales. It shows seasonal (Garcia-Lafuente et al., 2002a; Garrett et al., 1990) and inter-annual variability, sub-inertial (O(10 days)) changes driven by winds and, mainly, by atmospheric pressure differences between the Atlantic Ocean and the Mediterranean Sea (Candela et al., 1989; Garcia-Lafuente et al., 2002b) and diurnal and semidiurnal variations due to strong tidal currents, which interact with the topography of the strait and have marked influence on the mean flow.

Tidal currents in the strait have been extensively studied by analyzing observations collected over the last decades, most of them in the strait contraction area. The first description of the complicated tidal pattern was reported by Lacombe and Richez (1982) using data from the early sixties, although it was the experimental effort of the Gibraltar experiment in the mid-eighties that allowed for the investigation of the tidal currents with much greater detail. Using sea level records from different coastal stations, García Lafuente et al. (1990) first described the structure of the barotropic tide (sea level oscillation) and showed that the amplitude of the prevailing semidiurnal constituents diminishes more than 50% from the western to the eastern end of the strait and has little cross-strait structure. Candela et al. (1990) confirmed this pattern and described the tidal velocity field in some locations of the strait, particularly in the Camarinal sill section (Fig. 1). These authors found that, at tidal frequencies, the along-strait pressure gradient is mainly balanced by the acceleration of the flow, while the cross-strait balance tends to be geostrophic. Ten years after a new experimental effort was carried out during the Canary Islands Azores Gibraltar Observations (CANIGO Project, 1996–98). Several moorings were deployed in the strait to monitor the exchange and address its seasonality. An upward-looking ADCP installed in CS provided observations to study the vertical structure of the tidal currents with a high vertical resolution (Tsimplis, 2000). García-Lafuente et al. (2000) analyzed in detail the tide in the eastern part of the strait and Baschek et al. (2001) estimated the transport in this section using a tidal inverse model.

All these works focused on the main sill of Camarinal and on the eastern strait due to their demonstrated role on the hydraulical control of the exchange flows (Armi and Farmer, 1985). There are, however,

* Corresponding author. Tel.: +34 952132849; fax: +34 952131355.
E-mail address: antonio.sanchez@ctima.uma.es (A. Sánchez-Román).

0924-7963/$ – see front matter © 2012 Elsevier B.V. All rights reserved.
doi:10.1016/j.jmarsys.2012.02.011

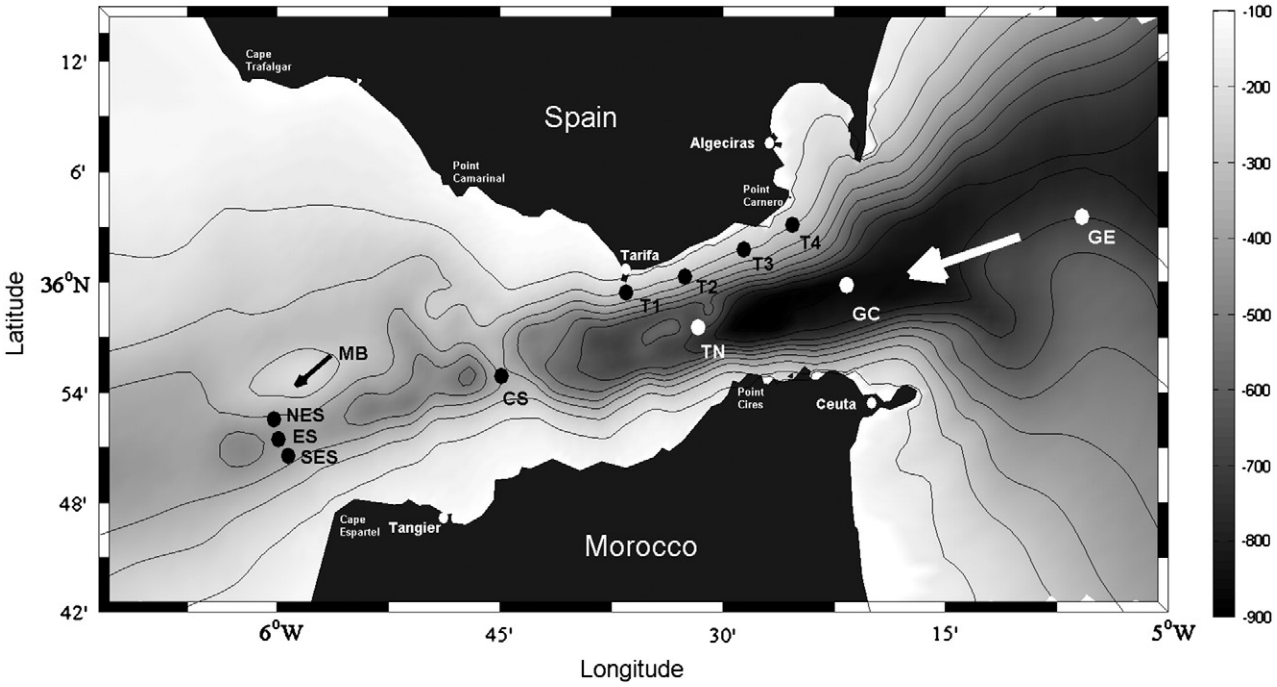

Fig. 1. Map of the Strait of Gibraltar showing the bathymetry (m) and the location of the stations. The topographic features shown are Espartel sill (ES), Camarinal sill (CS) and Tarifa narrows (TN). MB is the submarine ridge of Majuan Bank, which divides the Espartel section into two channels. NES and SES indicate the location of the auxiliary deployments in the main channel. GC and GE correspond to observing stations used in Sánchez-Román et al. (2009) that have been employed to construct the along-stream tidal maps. The white arrow indicates the direction of the flood tide.

other key places in the strait that deserved further attention. In late 2004, an oceanographic station was deployed at the sill of Espartel (ES, Fig. 1) west of CS with the aim of monitoring the Mediterranean outflow and its variability. This section, which has a complex topography due to the presence of the submarine ridge of Majuan Bank (Fig. 1) that divides the outflowing cross-section in two channels, represents the main gateway of the Mediterranean outflow. The observations at ES were already used by Sánchez-Román et al. (2008a) to describe the vertical structure of tidal currents in the main channel of this section, although a further investigation about the role played by this site in the tidal dynamics and associated transports in the strait is still lacking. These observations also indicate that the sill exerts hydraulic control over the outflow more than 96% of the time and the control is only lost for short periods of the ebb tide in the most energetic spring tides (Sánchez-Román, 2008b; Sannino et al., 2009), which makes ES suitable to monitor the Mediterranean outflow.

The present study has three main objectives, all of them aiming at providing a more complete description of tidal dynamics through the Strait of Gibraltar. The first objective is to investigate, for the first time, seasonal variability of tidal currents at the western strait by means of long velocity records available in ES. The second objective is to carry out a joint analysis of these data and other historical observations from other sites along the axis of the strait to depict a reliable pattern of the along-strait spatial variability of the tides in terms of the tidal transport. A first attempt to describe this pattern was made by García-Lafuente et al. (2000) using transports computed at the Eastern Exit of the strait and at CS. This work extends this analysis to the whole length of the strait by including the ES data in the western boundary of the area. The last objective of the paper is to investigate the cross-strait spatial variability of the flow at ES section and in the contraction area using recent observations with the aim of searching for dynamical connections between inshore and offshore tidal currents.

The paper is organized as follows: Section 2 describes the data and data processing. Section 3 addresses seasonality of tidal currents at ES. Section 4 discusses the along-strait spatial variability of tidal transports. Section 5 addresses the cross-strait spatial variability of the tidal currents and Section 6 discusses our results and summarizes the main findings.

2. Data and data processing

2.1. Datasets

The bulk of data come from the ES station (see Table 1 for details) in the main channel of the Espartel section. The station consists of an upward-looking moored ADCP at 345 m depth (15 m above seafloor) that resolves 40 bins, each 8-meter thick, and provides horizontal velocity at 40 levels every 30 min. This work analyzes the period from October 2004 to December 2009. Two auxiliary stations, equipped with up-looking ADCPs were deployed north (NES) and south (SES) of the ES station (Fig. 1) to describe the cross-structure of the outflow. It is important to remark that these stations were not deployed simultaneously (Table 1). Data collected by another ADCP at CS from January to April 2006 have been also used. The instrument profiled the horizontal velocity in 8 m bins between 44 and 260 m depth with a sampling interval of 30 min. Finally, data from four locations (T1 to T4 in Fig. 1) on the continental shelf break of the Spanish coast were collected by upward-looking ADCPs between May 2009 and April 2010 (see details in Table 1). The lines were placed along the 100 m isobath and the horizontal velocity was monitored in 2 m bins between the sea surface and 90 m depth with a sampling interval of 2 or 3 min (Table 1).

2.2. Data processing

2.2.1. Sequential harmonic analysis

The long record at ES has been used to investigate the time variability of harmonic constants. Classical harmonic analysis (Foreman, 1978; Pawlowicz et al., 2002) was performed to calculate tidal ellipses of the main diurnal (O_1 and K_1) and semidiurnal (M_2 and S_2) constituents. The dataset was divided in 3-month length sub-series and submitted to harmonic analysis to investigate the year-round variability of the harmonic constants. The sub-series overlapped 20 days to smooth

Table 1
Location and characteristics of the mooring lines.

Mooring line (bottom depth−m)	Instrument (frequency−KHz)	Latitude (N)	Longitude (W)	Bins (size−m)	Length series (days)	Sampling rate (min)	Covered period (day/month/year)
NES (341)	ADCP (150)	35° 52.65′	5° 58.46′	28 (8)	64	30	08/10/08–11/12/08
ES (360)	ADCP (75)	35° 51.70′	5° 58.60′	40 (8)	1919	30	30/09/04–31/12/09
SES (321)	ADCP (150)	35° 50.56′	5° 58.40′	35 (8)	128	30	30/10/07–06/03/08
CS (290)	ADCP (150)	35° 54.63′	5° 44.79′	28 (8)	92	30	26/01/06–28/04/06
T1 (100)	ADCP (190)	35° 59.59′	5° 35.73′	35 (2)	36	2	26/05/09–01/07/09
T2 (100)	ADCP (190)	36° 00.76′	5° 31.55′	32 (2)	100	3	01/07/09–09/10/09
T3 (100)	ADCP (190)	36° 01.64′	5° 28.00′	38 (2)	90	2.5	09/10/09–07/01/10
T4 (100)	ADCP (190)	36° 02.91′	5° 25.72′	38 (2)	76	2.5	05/02/10–22/04/10

transitions between segments. According to the Rayleigh criterion, 3 months is not enough to separate the contributions of pairs S_2–K_2 and K_1–P_1, which demand a length of at least 6 months. Therefore, S_2 and K_1 harmonic constants estimated from three-month series will be affected by their non-resolved companions. To solve this problem, harmonic analysis was applied to the whole ES series to obtain the amplitude ratio and the phase difference of these constituent pairs that are necessary to make inference in the three-month series in order to extract the S_2 and K_1 contributions as explained in Foreman (1978), or Pawlowicz et al. (2002).

2.2.2. Non simultaneous records at Espartel

The analysis of simultaneous data throughout the entire ES channel is not possible since the auxiliary mooring lines NES and SES were not deployed simultaneously. To make them comparable, we first extracted two sub-series of velocity at ES during the periods of NES and SES observations, respectively. Each sub-series provided a set of harmonic constants that were inter-compared to identify differences between both periods. These differences were taken into account in order to correct the results of the harmonic analysis in NES for the bias arising from the lack of simultaneity with data at SES and to make the results of both harmonic analyses comparable. The procedure was as follows.

Vertical distributions of amplitude (A_z) and phase ($\varnothing_z$) obtained from harmonic analysis in ES can be expressed as

$$\begin{aligned} X_{ES}(z)^{i,j} &= A_z^{i,j}\cdot cos(\varnothing_z)^{i,j} \\ Y_{ES}(z)^{i,j} &= A_z^{i,j}\cdot sin(\varnothing_z)^{i,j} \end{aligned} \tag{1}$$

where $X_{ES}(z)$ and $Y_{ES}(z)$ are the Cartesian projections of the amplitude/phase (at depth z) of the tidal constituents j and $i=1,2$ which are the two time periods considered (October 2007 to March 2008 and October to December 2008). The factors

$$\begin{aligned} FX_{ES}(z)^j &= \frac{X_{ES}(z)^{1,j}}{X_{ES}(z)^{2,j}} \\ FY_{ES}(z)^j &= \frac{Y_{ES}(z)^{1,j}}{Y_{ES}(z)^{2,j}} \end{aligned} \tag{2}$$

are the ratios of these projections for constituent j at the two different time periods, which ideally should be 1. Departures from this value would be ascribed to the time variability we are interested to correct. On the other hand, the ratios at ES are expected to be representative for the entire cross section of Espartel because they are more linked to time than to spatial variability. Therefore, these ratios can be used to estimate harmonic constants at NES or SES stations when observations are lacking if harmonic constants at ES are known from measurements collected in other different period. In our case, the harmonic constants at NES during October 2007 to March 2008 (period of SES observations) have been estimated from harmonic constants obtained at NES from October to December 2008 corrected by the ratios computed at ES from data collected in both time periods:

$$\begin{aligned} X_{NES}(z)^{1,j} &= FX_{ES}(z)^j\cdot X_{NES}(z)^{2,j} \\ Y_{NES}(z)^{1,j} &= FY_{ES}(z)^j\cdot Y_{NES}(z)^{2,j}. \end{aligned} \tag{3}$$

Amplitude and phase are then recovered:

$$\begin{aligned} A_{NES}(z)^{1,j} &= \sqrt{\left[X_{NES}(z)^{1j}\right]^2 + \left[Y_{NES}(z)^{1j}\right]^2} \\ \Phi(z)^{1,j} &= \arctan\frac{Y_{NES}(z)^{1,j}}{X_{NES}(z)^{1,j}}. \end{aligned} \tag{4}$$

The performance of this procedure has been tested using data from the SES series, which is longer than the NES series. Three subsets of a synodic month length (29.53 days) were extracted from the SES series and three other simultaneous sub-series were extracted from the ES series. The ratios (2) obtained at ES for the first and second sub-series were employed to infer the harmonic constants of M_2 and O_1 at SES during the period of the second sub-series using the computed harmonic constants of the first sub-series. The inferred constants were compared with the constants computed directly from the data of the second sub-series to find that both sets of constants were highly correlated (0.98 for M_2 amplitude, 0.97 for M_2 phase; 0.97 for O_1 amplitude, 0.94 for O_1 phase). The procedure was repeated for the second and third sub-series with the same satisfactory results, which supports the use of this procedure to infer harmonic constants at NES during the period October 2007 to March 2008 when data at ES and SES are available. Inferred M_2 amplitude highly correlates (0.95) with that observed at NES during the period October to December 2008 (0.85 for M_2 phase). It translates on a mean amplitude difference between both vertical velocity profiles of 0.04 ± 0.02 m s^{-1} ($13\pm4.74°$ for the phase) resulting from the temporal variation of tidal flow. The inferred constants overall differ from those computed during the second period by around 12%, which is ascribed to the seasonality and interannual variability of the tidal currents.

2.2.3. Interface depth at Espartel

Tidal currents in the upper Atlantic layer at Espartel are larger than the velocity of the mean flow (about 0.15 m s^{-1} on average) and reverse the Atlantic inflow almost every tidal cycle (Sánchez-Román et al., 2009). For this reason, the concept of an interface of null along-strait velocity separating Atlantic and Mediterranean flows is not applicable at tidal frequencies and the interface depth must be estimated in another way. Alternatively we use the depth of the maximum vertical shear of horizontal velocity, which is well resolved by ADCP velocity profiles, as a proxy of the interface depth (Tsimplis, 2000). Sánchez-Román et al. (2009) applied this procedure to compute the interface depth at ES and showed that the surface of maximum shear is at a mean depth of 230 m, 40 m below the surface of null velocity computed for subinertial flows whose mean depth is 190 m. Thus the interface depth at tidal frequencies, which is needed to calculate tidal transports in Section 4, has been computed by

adding 40 m to the depth of maximum vertical shear (see Sánchez-Román et al., 2009 for more details).

3. Seasonal variability of tidal currents

The percentage of energy associated with tides (PET hereinafter) has been used as a tool to assess the importance of tidal signal on the total current. PET is computed as the ratio of the variance explained by the harmonic analysis and the variance of the original series. The former is computed from the series synthesized with the harmonic constants of the constituents that have signal-to-noise ratio greater than 3 in the harmonic analysis (Pawlowicz et al., 2002).

Fig. 2.a shows that PET at ES is not evenly distributed along the water column. Maximum values above 0.9 are found in the upper Atlantic layer where tidal currents prevail over the mean flow. Minimum values are found close to the bottom as a result of friction and also in the lower layer below the mean interface, that is, in the transitional region between the Mediterranean and Atlantic waters, which is considered as a layer itself (Bray et al., 1995). In this layer, which extends vertically from 160 to 250 m depth and undergoes noticeable vertical mixing (Sánchez-Román, 2008b), PET is reduced by around 35%.

In addition to this vertical pattern observed during the whole period, PET changes during the year, showing minimum values in autumn–winter. Since PET is a percentage, this reduction can stem from the enhancement of subinertial currents, from a weakening of tidal currents or both. To address this issue, the subinertial outflow has been computed according to

$$OUT(t) = \int_b^{h(t)} \langle u(z,t) \rangle W(z) dz \quad (5)$$

where $<u(z,t)>$ is the along-strait subinertial velocity profile, W is the channel width at depth z, b is the bottom depth and $h(t)$ is the depth of the interface, which coincides with the surface of null velocity for subinertial flow. The subinertial velocity has been obtained by applying an 8th order low-pass Butterworth filter to the original observations with pass and stop frequencies $f_1 = 0.0263$ cph and $f_2 = 0.0357$ cph. This computation implicitly assumes that a single velocity profile is representative of the entire channel width and it ignores any cross-channel structure of the flow.

The subinertial flow is enhanced in winter (Fig. 2.b), an expected result ascribed to the sensitivity of the exchange flow to the passage of atmospheric systems over the Mediterranean basin (Garcia-Lafuente et al., 2002b), which are more frequent and intense during this season. Therefore, subinertial flow enhancement does contribute to the PET reduction in autumn–winter. On the other hand, the sequential harmonic analysis carried out to investigate the variability of the harmonic constants (Fig. 3.a) shows an actual weakening of M_2 tidal currents in winter as well, which suggests that both mechanisms contribute to the diminution of the PET observed during the winter.

Maximum values of M_2 semimajor axis are found in summer (vertical arrows in Fig. 3.a). During the first 3 years the phase increased by around 30° in this season as well (Fig. 3.b), a situation that was not met in years 2008 and 2009. The vertical pattern shows maximum tidal velocity and phase around 220–250 m depth, the same depth as the surface of maximum shear. It can be explained by the coupling of the interface dynamics and the tidal flow: during the flood (west-going) tide, tidal current increases the Mediterranean outflow and raises the interface, transferring kinetic energy to the lower layer mean flow. When the tidal flow reverses, the interface sinks and tidal current increases the Atlantic inflow at approximately the same depth as the previous flood had increased the outflow. The final result is the enhancement of tidal signal at this level, which is reflected in the harmonic analysis. The mechanism does not depend on any particular constituent and therefore the increase of amplitude in the 220–250 m depth range is a common feature of all constituents.

An increase of the M_2 phase of 30 to 60° is also observed below the mean interface at the same depth range (Fig. 3.b). It implies downward phase propagation above the depth of the local maximum and upward propagation below that depth. According to the linear theory of internal waves in a continuously stratified flow, the group velocity (that is, the energy) and the phase have vertical propagation of different signs at semidiurnal frequencies because M_2 frequency verifies $N > \omega_{M2} > f$, with N the buoyancy frequency and f the Coriolis parameter (Bruno et al., 2002; LeBlond and Mysak, 1978). Therefore the energy propagates upward (downward) from the depth of maximum phase toward the sea surface (sea bottom), a propagation that agrees

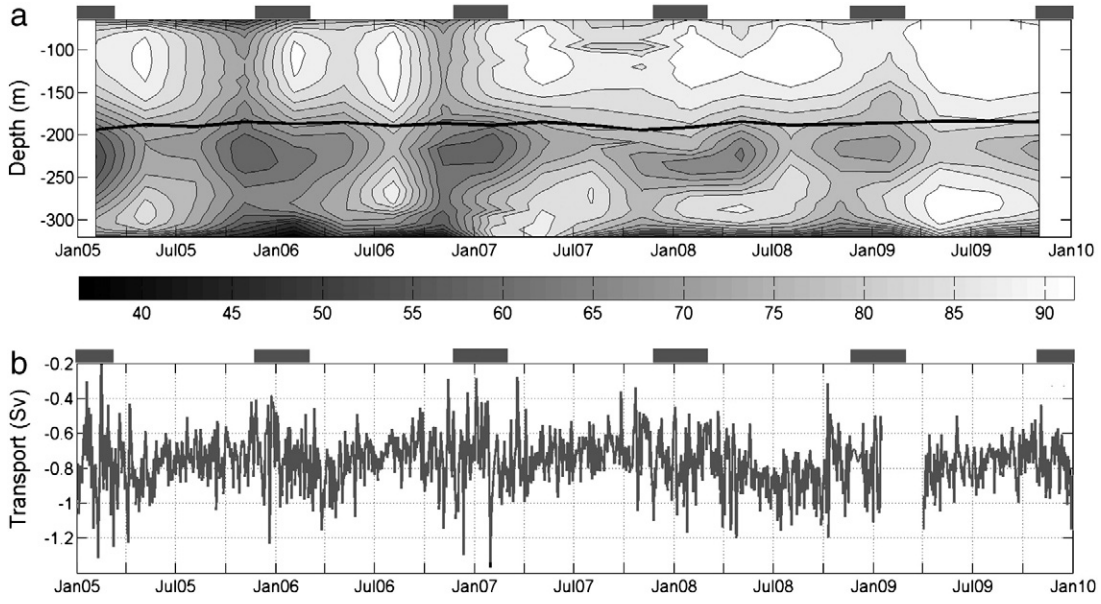

Fig. 2. (a) Percentage of energy explained by tides in the velocity records collected at ES. Black line is the interface calculated from the surface of the maximum vertical shear of the horizontal velocity at tidal frequencies (see text for details). (b) Low frequency (subinertial) transport in the Mediterranean layer. Black small rectangles on top denote the winter periods.

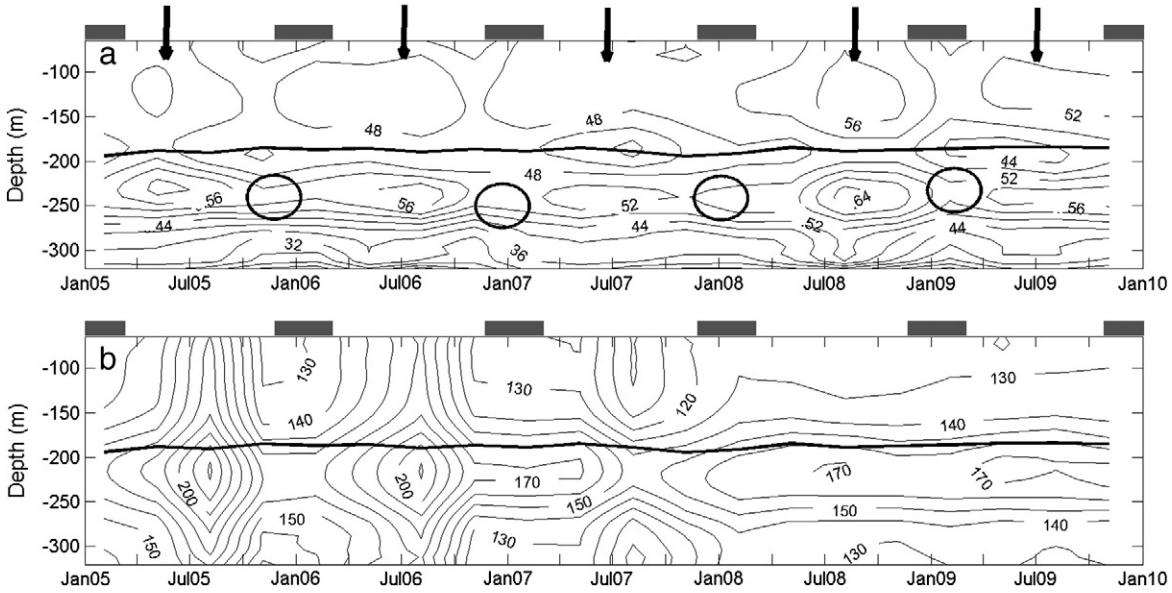

Fig. 3. Temporal variability of M_2 harmonic constants at ES. (a) Semimajor axis (cm s^{-1}), (b) phase (degrees). The black line is the interface calculated as in Fig. 2. Black small rectangles on top denote the winter periods and arrows and circles indicate the periods of maximum (around July) and minimum (around January) amplitudes, respectively.

with the fact that the maximum M_2 amplitude is found at the same depth.

4. Tidal transport

4.1. Transport computations

The first attempt to compute tidal transports in the Strait of Gibraltar was made by Bryden et al. (1994) at CS, who found M_2 tidal transport amplitude of 2.3 Sv at 151° in the Atlantic layer and 1.3 Sv at 144° in the Mediterranean layer. In the eastern side of the strait, García-Lafuente et al. (2000) computed a M_2 signal of 0.33 Sv at 184° and 2.78 Sv at 130° in the Atlantic and Mediterranean layers, respectively. Both estimates were carried out using a salinity surface as interface. Even though the amplitude of M_2 signal in the Atlantic layer at CS provided by Bryden et al. (1994) is probably overestimated, a fact acknowledged by the authors of that paper themselves and corroborated later on by García-Lafuente et al. (2000) and Tsimplis and Bryden (2000), the numbers above indicate the strong divergence of the tidal transport in each layer, which is linked to the spatial variability of the tides (see Figs. 3 to 6 in Sánchez-Román et al., 2009).

New estimates of tidal transport at CS and ES sections have been done in this work with the ADCP observations collected at both sills. Mediterranean layer transport has been estimated from Eq. (5) using the original time series and the interface depth calculated according to the procedure described in Section 2.2. The harmonic constants from these series of tidal transport along with the results obtained by García-Lafuente et al. (2000) are presented in Table 2 for the most important diurnal and semidiurnal constituents. Harmonic constants of the Mediterranean layer tidal transport are reliably estimated at ES using the velocity profiles but they are not for the Atlantic layer because of the widening of the strait in the surface layer (Fig. 1) and the lack of reliable observations within this layer. Nevertheless a reasonably good estimate is readily done using the constancy of the barotropic tidal transport. These indirect estimations of harmonic constants at ES are included in Table 2 as well. Except for the values in the Atlantic layer in the ES section, the numbers on this table come from series spanning several months and they can be considered representative of the mean tidal flows (for comparison purposes, at least) due to the stationary character of tides, even when transports in GC were computed from observations collected some years before. The fact that the new estimate of M_2 in the Mediterranean layer at CS agrees well with the value reported by Bryden et al. (1994) corroborates this assumption.

The total (barotropic) tidal transport is computed by adding up the transport in both layers. With the values given by García-Lafuente et al. (2000), the M_2 and S_2 barotropic signals in GC are 3.0 Sv at 135° and 1.1 Sv at 166°, respectively. Using the values obtained in this study, the corresponding values in the CS section are 3.1 Sv at 138° for M_2 and 1.1 Sv at 177° for S_2, which agree quite well with those at GC, verifying the expected volume conservation for the total barotropic tide.

4.2. Along-strait dynamics of the tidal transport

The estimated transports in Table 2 are used here to describe the along-strait spatial variability of tidal transports in the Atlantic and Mediterranean layers. The striking point in Table 2 is the steady decrease of transport amplitude in the Mediterranean layer from east (GC) to west (ES) for all constituents, which is more noticeable for the prevailing

Table 2
Tidal transports associated to the main tidal constituents, obtained from the harmonic analysis performed to the transport time series. Values in the Atlantic layer at ES have been inferred from the constancy of the barotropic flow, as explained in the text.
Harmonic constants at GC are from García-Lafuente et al. (2000).

	Espartel section (ES)				Camarinal section (CS)				Eastern section (GC)			
	Atlantic		Med.		Atlantic		Med.		Atlantic		Med.	
	A (sv)	Φ (deg)	A (sv)	Φ (deg)	A (sv)	Φ (deg)	A (sv)	Φ (deg)	A (sv)	Φ (deg)	A (sv)	Φ (deg)
M_2	2.80	133	0.35	162	1.88	139	1.25	137	0.33	184	2.78	130
S_2	0.97	173	0.13	189	0.56	178	0.56	166	0.17	190	0.90	161
O_1	0.48	82	0.14	34	0.42	99	0.28	29	0.22	48	0.58	331
K_1	0.59	92	0.12	114	0.47	89	0.24	110	0.22	190	0.57	47

semidiurnal constituents and particularly for M_2. The opposite behavior is found in the Atlantic layer, where amplitude increases monotonically from east to west. Phases of semidiurnal constituents also show such monotonic characteristic. This behavior was reported by García-Lafuente et al. (2000) between the eastern exit of the strait and the main sill of Camarinal and the analysis here not only confirms this result but also extends it to the western exit of the strait. Between GC and CS, the amplitude of M_2 transport in the Mediterranean layer is reduced by more than 50% while it is nearly 6 times greater in the Atlantic layer at CS (Table 2). A very clear transfer of the tidal signal from the Mediterranean to the Atlantic layer takes place between GC and CS during the flood tide and vice-versa during the ebb tide. This fact led Bray et al. (1990) to propose the conceptual model of a membrane-like interface between CS and GC sections whose role would be the transfer of the tidal signal from one layer to the other. Phase difference between these locations in the Atlantic layer indicates that tidal transport propagates from CS to GC, a fact that is ascribed to the strong baroclinic nature of the internal tide. An inspection of values in Table 2 indicates that the same behavior applies between CS and ES sections.

The two-layer sketches presented in Fig. 4 illustrate key aspects of the tidal dynamics in the strait and explain the aforementioned divergences. Fig. 4.a represents the hypothetical mean exchange and mean interface position in the absence of tidal forcing. Tidal transports associated with M_2 within each layer (small two-headed arrows with size proportional to the transport, which is indicated by the numbers beside) and the total barotropic transport (large arrows with numbers inside) have been included for ES, CS and GC sections (see Fig. 1 for locations). Notice that M_2 transport by itself (3.1 Sv) would reverse the mean flow, which is around 0.8 to 1 Sv in each layer (Baschek et al., 2001; Garcia-Lafuente et al., 2002a; Sánchez-Román et al., 2009), if it were equally distributed among both layers. This is not the case at the strait's boundaries because most of the tidal flow moves through the passive, slow-flowing layer (Mediterranean layer in the east, Atlantic layer in the west), making them reverse periodically. At these boundaries, however, the tidal transport in the active, fast-flowing layers is insufficient to reverse the total flow. In CS the amplitude of M_2 in any layer is greater than 1 Sv and, except for some neap tides, the total flow in each layer reverses during part of the tidal cycle.

Fig. 4.b sketches the flow during flood tide (thick gray line in the sea level graph) that implies westward barotropic tidal transport (thick arrow beside the graph). At this time, the flow is hydraulically controlled at CS and only a limited volume of the west-going tidal flow that has flown through GC is able to surpass the sill, the rest remaining trapped between both sections. Consequently, the interface is pushed upward and forces water in the Atlantic layer to move away from the area. Part of it moves eastward, thus reducing the amplitude of tidal currents in the upper layer at GC, but most of it goes on to the west, transferring the signal from the Mediterranean to the Atlantic layer. Some tidal flow can be transferred cross-strait reaching the continental shelf of both the Spanish and Moroccan coasts and promoting some coastal recirculation. This topic will be addressed in the next section. At the ES section, west of CS, the Mediterranean flow is also hydraulically controlled. In fact, the hydraulic control in ES is more permanent than in CS (Sánchez-Román, 2008b; Sannino et al., 2007, 2009) and the reduced fraction of the tidal transport crossing CS is not even able to overflow ES. Consequently, the water accumulates in the Tangier basin forcing the flow to change to subcritical and originating the well-known internal hydraulic jump downstream CS (Armi and Farmer, 1988; Sanchez-Garrido et al., 2008, 2011). Once more the interface is pushed up displacing the Atlantic water above toward the Atlantic Ocean and completing the transfer of the large tidal signal that is observed in the lower layer in the east to the upper layer in the west. A first guess of the interface vertical excursion in the Tangier basin is obtained by integrating the equation

$$S\frac{\partial \eta}{\partial t} = Q_{2,E} - Q_{2,C} \tag{6}$$

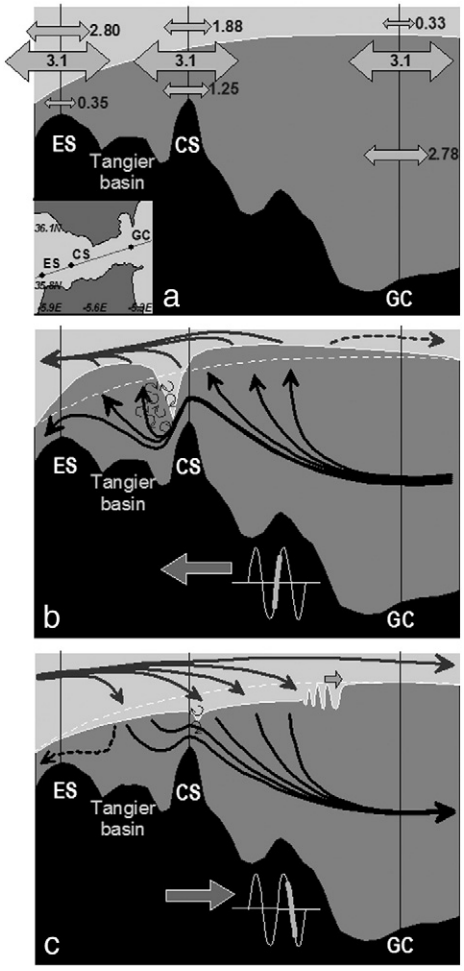

Fig. 4. Two-layer sketch to explain tidal transport divergence in each layer. (a) Plate of the mean exchange with indication of M_2 tidal transport. The mean flow of around 0.8 Sv in each layer has not been indicated to prevent the figure from being overcrowded with numbers. (b) Illustration of the flood tide (barotropic tidal current toward the Atlantic Ocean). (c) The same for ebb tide (tidal current toward the Mediterranean). See text for a more detailed explanation.

where η is the interface depth, S is its horizontal area assumed constant and equal to the area at its mean depth in the inter-sill region (160 m), and $Q_{2,E}$ and $Q_{2,C}$ are the tidal transports in the Mediterranean layer through the ES and CS sections, respectively. The equation, which is applicable to any constituent, gives a vertical excursion of around 75 m for M_2 (35 m for S_2), which is an important fraction of the water depth in the Tangier basin (~500 m).

During ebb tide the situation reverses, but the interpretation is rather similar. The main difference is the flooding of the hydraulic control in CS by the end of the flood tide when the tidal current weakens and the subsequent release of the internal jump that propagates as an internal bore with the associated short-wavelength internal wave packet to the east (Fig. 4.c). The flooding of CS control allows the accumulated Mediterranean water in the Tangier basin to flow eastward, thus reversing the flow in this layer at CS, although part of the water keeps on flowing westward, smoothing out the amplitude of tidal currents at ES in this layer. The Mediterranean water accumulated between CS and GC in the previous flood evacuates toward the Mediterranean through GC, a process favored by the hydraulic control in Tarifa narrows that prevents the large volume of Atlantic water moving to the east during the ebb tide to cross the control section. As this water accumulates between CS and GC, it pushes down the interface and forces the Mediterranean water below to flow back

toward the Mediterranean Sea, thus transferring the tidal signal to the lower layer.

5. Cross-strait variability

The velocity observations at stations T1 to T4 in the contraction area and at NES and SES in the Espartel section are analyzed next to depict some characteristics of the cross-strait structure of the flow. It is a relevant issue as it helps improve the estimates of flows computed from observations made at a single station, usually located in the central part of the strait, which assumes uniformity across the whole section.

5.1. The strait contraction

Fig. 5 presents the spatial distribution of amplitude and phase of M_2 along the central part of the strait, adapted from Sánchez-Román et al. (2009), and along the continental shelf break off Tarifa, obtained from moorings T1 to T4. As explained in Sánchez-Román et al. (2009), the amplitude of M_2 is maximum at CS, the bottleneck of the strait, and decreases toward the eastern and western ends (Fig. 5.a), while the phase presents anti-symmetric behavior with respect to the sill: they are higher in the fast-flowing layers where the mean flow is stronger than tidal currents, and lower in the passive layers. The distribution of near-shore amplitudes and phases (Fig. 5.a.2, b.2) resembles the pattern in the central section at the same longitude (Fig. 5.a.1, b.1). In both cases, semimajor axis decreases markedly toward the east with larger gradient in the offshore section. Near-shore, friction reduces the amplitude near the bottom and distorts the barotropic shape exhibited by the semimajor axis in the rest of the water column. Friction would also be responsible for the slightly smaller values of the vertically averaged amplitudes. At the easternmost part of the small domain, where the strait widens due to the presence of the embayment of Algeciras (see T4 location in Fig. 1), M_2 amplitude has been reduced to less than 20 cm s^{-1} in both sections, which is around 30% (near-shore) and 25% (central) of the values at the western part of the domain.

Phases show local maximum near 5.45° W and increase upward (Fig. 5.b.1 and b.2), which would imply downward propagation of the energy at M_2 frequency. Horizontally, the phase increases eastward showing the progressive nature of the internal tide that propagates to the east. This progressive nature is much less evident in the near-shore section where the mean value is also around 70° smaller, an important difference that implies a time lag of more than 2 h. Near-shore tidal currents lead currents in the center of the channel, which generates cross-strait gradient of tidal currents larger than those produced by the small cross-strait reduction of tidal amplitudes described above.

These noticeable features are likely linked to the internal divergences of tidal transports discussed in the previous section: the existence of hydraulic control in CS during the flood tide forces the accumulation of Mediterranean water in the narrow part of the strait (Fig. 4.b). In a 2-D model, the accumulation pushes the interface upward and forces the water in the Atlantic layer above move backward or forward, but in a more realistic 3-D model coastal recirculation is very likely to occur. The fact that at a given depth and longitude the near-shore tidal currents lead by 2 h the tidal currents offshore suggests that part of the displaced Atlantic water flows along the coastal area first and then through the rest of the section. Therefore, significant

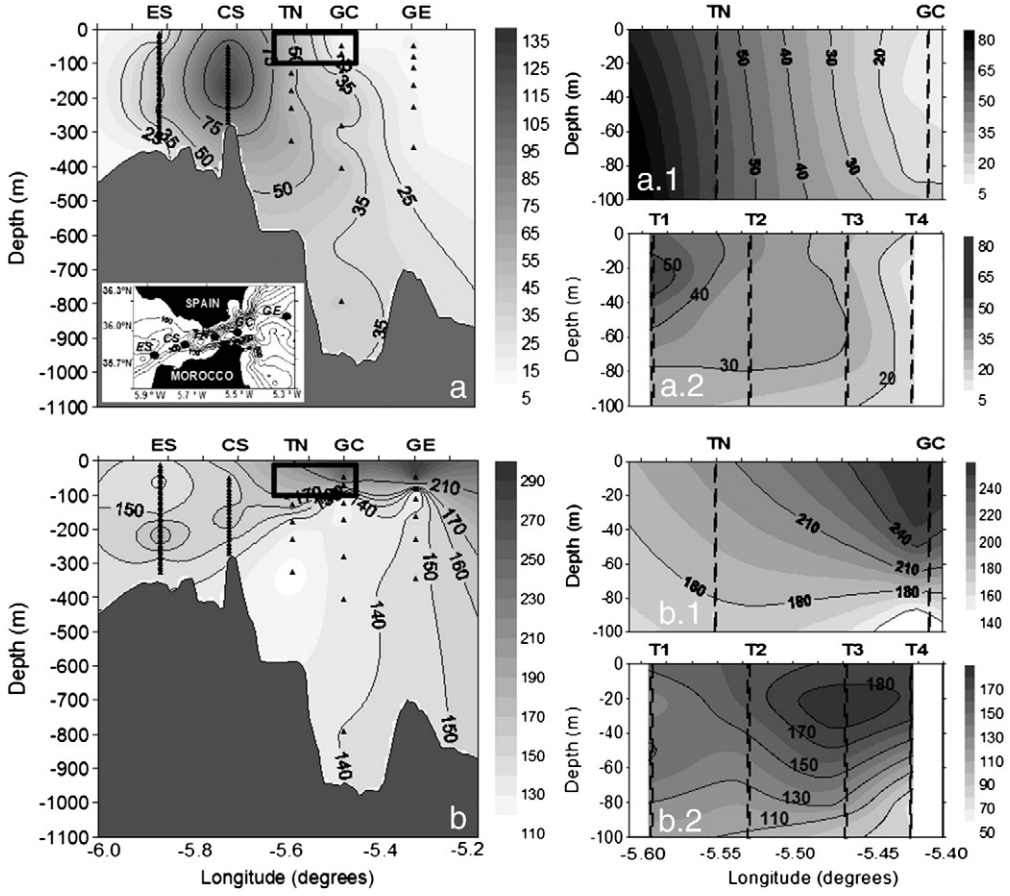

Fig. 5. Tidal maps of the along-strait velocity for M_2 constituent. Panels (a) and (b) represent the amplitude (cm s^{-1}) and phase (degrees) along the central axis of the strait. Solid triangles indicate the sampling points. Panels a.1 and b.1 enlarges the area inside the black rectangles in panels a and b. Panels a.2 and b.2 denote the M_2 amplitude (cm s^{-1}) and phase (degrees) obtained from the data collected along the continental shelf of the Spanish coast in the same region as in a.1 and b.1 panels. Dashed vertical lines indicate the observation sites. Notice that the phase range in b.1 and b.2 is not the same.
Panels a and b are adapted from Sánchez-Román et al. (2009).

cross-strait circulation and some variability in along-strait flows are expected to occur driven by the tidally-forced vertical displacement of the interface. Moreover, near-shore frictional effects also contribute to the non-uniformity of the along-strait flow in the cross-section.

5.2. Espartel section

The inferred harmonic constants at NES during the period of SES deployment have been used in Fig. 6 to show the spatial pattern of tidal currents at the Espartel section. Fig. 6.a,b shows the contours of the semimajor axis of M_2 and K_1, respectively, and Fig. 6.c,d the phases. These records were collected in winter; according to the harmonic constant seasonality reported earlier, tidal amplitudes would have smaller values than if it comes from records collected in summer. In agreement with the results presented in Section 3, spatial maximum amplitudes are observed at mid-depths below the mean interface, which slopes up from 200 m in the south to 170 m in the north due to Earth rotation. A second maximum of M_2 amplitude is visible in the upper part of the water column above the interface (the lack of data above 100 m depth prevents us from depicting the near-surface spatial extension and shape of this maximum). In the Mediterranean layer, between 200 and 270 m, the M_2 amplitude shows a marked horizontal gradient (Fig. 6.a) with the minimum value close to the northern boundary roughly in the same place where phase is maximum (Fig. 6.c). This phase maximum is a feature that extends across the channel whose physical interpretation was given in Section 3 in terms of the linear theory of internal waves: vertical energy propagation from this region upward and downward, opposite to the vertical phase propagation. The phase also shows a horizontal gradient, with values around 30° lower in the south, which implies that the maximum of tidal currents occurs 1 h earlier in the south. These horizontal gradients of amplitude and phase generate horizontal shear (i.e. relative vorticity) of the same sign, although the amplitude gradient is the major contributor. In the Atlantic layer the distribution of phase is nearly independent of the cross-strait coordinate and the amplitude exhibits a very low gradient as well, both facts suggesting a rather horizontally homogeneous M_2 tidal flow.

Amplitude of K_1 (Fig. 6.b) resembles the distribution of M_2 in the lower layer with marked gradients and greater values in the south. The spatial pattern above the interface is quite homogeneous. Phase (Fig. 6.d) changes quickly in the vertical axis as we move from the Atlantic to the Mediterranean layer (peak current nearly 2 h earlier in the former) and does not exhibit cross-channel variability. The spatial gradients of amplitude in the lower layer are probably due to the topographic conveying of the flow by the prominent seamount of Majuan Bank that outlines the northern boundary of the main channel of Espartel (Fig. 1). Topography displaces the tidal stream to the south and this mechanism acts in the same manner on every constituent, which would justify the similitude of K_1 and M_2 maps.

6. Summary and conclusions

A five year-long time series of velocity collected at ES has been analyzed to assess the relative importance of the tides on the total flow, its seasonal variability and its spatial structure with the help of two other auxiliary stations deployed north and south of the main station of ES. The percentage energy associated with tides (PET) reaches over 90% in the upper layer, suggesting a tidally driven flow in this layer, and diminishes markedly downward. Minimum values are close to the bottom due to frictional effects and in the transitional area between the Atlantic and Mediterranean waters. A seasonal signal with minimum PET in autumn–wintertime is observed all years due to the enhancement of subinertial currents and also to the weakening of M_2 tidal currents in this season (Figs. 2.b and 3.a).

The vertical structure of the tidal flow in ES exhibits maximum values of M_2 amplitude below the mean interface (Fig. 3.a) between 220 and 250 m. It is explained by the tidally-induced vertical displacement of the interface, which leaves this depth-range immersed in the Mediterranean layer during the flood tide (when the total current increases substantially toward the Atlantic) and inside the upper layer during the ebb tide (when the tidal flow reverses and increases the upper layer current toward the Mediterranean Sea). This mechanism favors the generation of enhanced signals for all tidal constituents independently of their frequencies. The mechanisms that modulate the

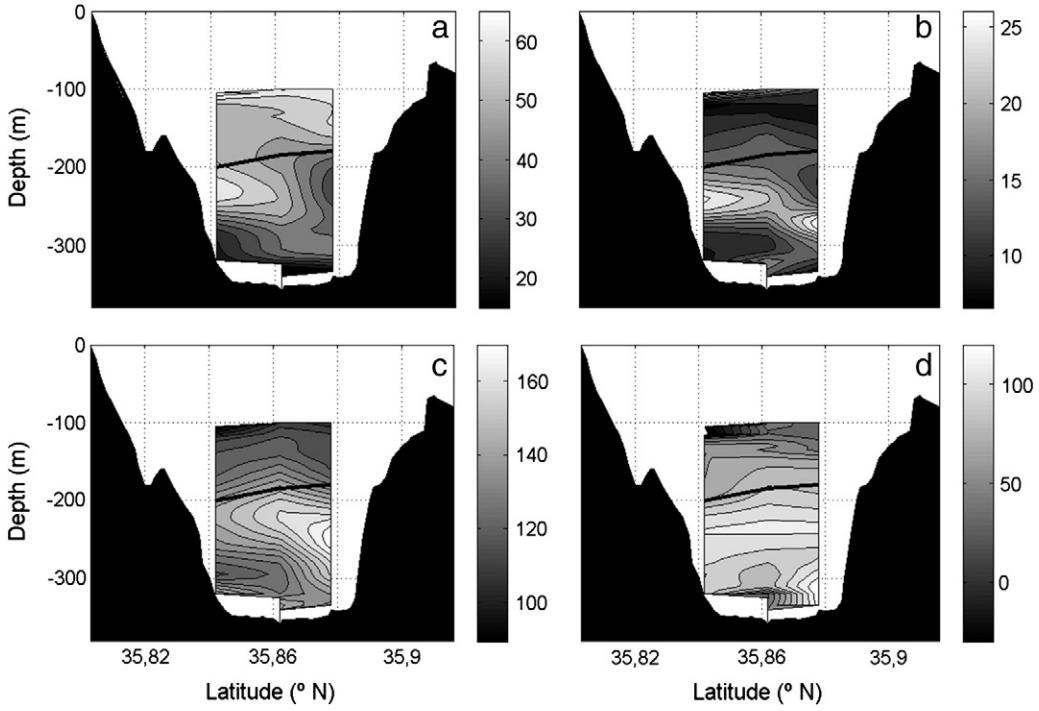

Fig. 6. Spatial distribution of tidal currents across the main channel of the Espartel section. Contours have been plotted using data from SES, ES and NES stations. Upper panels are amplitude (cm s^{-1}) for M_2 (a) and K_1 (b). Lower panels are phase (degrees) for M_2 (c) and K_1 (d). Black line represents the mean position of the interface.

along-strait dynamics also have impact on the cross-strait structure of the flows, which show maximum values of amplitudes and phases below the mean interface as well, reproducing the results obtained at the single station ES (Fig. 6). Amplitude and phase are not horizontally homogeneous but exhibit horizontal gradients that induce a horizontally sheared tidal flow, with larger values in the southern part of the channel. The pattern is probably driven by the topography that favors the southward displacement of tidal streamlines.

The definition of an interface at tidal frequencies based on the vertical shear of horizontal velocity has allowed for the computation of time series of instantaneous layer transports at ES and CS sections and their harmonic constants, which complement historical information on this topic reported by García-Lafuente et al. (2000) in GC (see Table 2). The results obtained in ES have been compared with transports re-computed at CS and those reported by García-Lafuente et al. (2000) to depict the along-strait tidal dynamics in terms of the internal hydraulics of the strait, which highlights the complexity of the internal tide. As a result, we have corroborated the pattern reported by those authors between CS and GC, which has been also extended to the sill of Espartel. While the total (barotropic) transport for each constituent is constant, Table 2 shows that it is not true for transports in each layer. Strong internal divergences take place between the different sections, which are responsible for vertical excursions of the interface as large as a hundred meter and also for the transfer of tidal signals between the Mediterranean and the Atlantic layers and vice versa. During flood tide, for instance, the transfer is achieved by hydraulic controls in the ES, CS and TN sections, which makes the interface rise and displaces the Atlantic water above toward both the Atlantic Ocean and the Mediterranean Sea, enhancing the tidal signal in the Atlantic side of the strait and reducing it in the Mediterranean one. A possibility that cannot be addressed by this conceptual model, which is independent of the cross-strait coordinate, is the coastal recirculation that would appear if part of the water displaced by vertical motion of the interface flows to the shores. A set of observations collected on the shelf break in the north shore strongly suggests that, actually, part of this evacuation is achieved as coastal countercurrents that lead by 2 h the tidal current in the central part of the channel.

Acknowledgments

Datasets analyzed in this work were collected within the frame of the Spanish-funded INGRES projects (REN03-01608/MAR, CTM06-02326/MAR, CTM2010-21229-C02-01/MAR) and Accion Complementaria CTM2009-05810/E as well as the FLEGER (RNM-3738) regional project. We are grateful to the Spanish Ministry of Science and Innovation and the Regional Government of Junta de Andalucía (Spain) for their financial support. ASR acknowledges a post-graduate fellowship from this ministry, and wants to thank Xavier Jofre for his review of the final version of the paper. We are also grateful to the crews of the R/Vs Odon de Buen and Francisco de Paula Navarro from the Instituto Español de Oceanografía for the help, assistance and well-done work during the deployment and recovering of the mooring lines in the often unfriendly environment of the Strait of Gibraltar. The authors are also thankful to two anonymous referees for the helpful comments and suggestions. This is the publication no. 2 from the CEIMAR Journal Publication Series. The ES monitoring station is part of the Mediterranean Sea monitoring network Hydro-Changes, sponsored by the CIESM.

References

Armi, L., Farmer, D.M., 1985. The internal hydraulics of the Strait of Gibraltar and associated sills and narrows. Oceanol. Acta 8, 37–46.
Armi, L., Farmer, D.M., 1988. The flow of Mediterranean water through the Strait of Gibraltar. Prog. Oceanogr. 21, 1–105.
Baschek, B., Send, U., García-Lafuente, J., Candela, J., 2001. Transport estimates in the Strait of Gibraltar with a tidal inverse model. J. Geophys. Res. 106 (C12), 31,033–31,044.
Bray, N., Winant, C.D., Kinder, T.H., Candela, J., 1990. Generation and kinematics of the internal tide in the Strait of Gibraltar. In: Pratt, L.J. (Ed.), The Physical Oceanography of Sea Straits. Kluwer Academic Publisher, Dordrecht, p. 477.
Bray, N.A., Ochoa, J., Kinder, T.H., 1995. The role of the interface in exchange through the Strait of Gibraltar. J. Geophys. Res. 100 (C6), 10755–10776.
Bruno, M., Alonso, J.J., Cózar, A., Vidal, J., Ruiz-Cañavate, A., Echevarría, F., Ruiz, J., 2002. The boiling-water phenomena at Camarinal sill, the Strait of Gibraltar. Deep Sea Res. Part II 49, 4097–4113.
Bryden, H.L., Candela, J., Kinder, T.H., 1994. Exchange through the Strait of Gibraltar. Prog. Oceanogr. 33, 201–248.
Candela, J., Winant, C., Bryden, H.L., 1989. Meteorologically forced subinertial flows through the Strait of Gibraltar. J. Geophys. Res. 94, 12,667–12,674.
Candela, J., Winant, C., Ruiz, A., 1990. Tides in the Strait of Gibraltar. J. Geophys. Res. 95, 7313–7335.
Foreman, M.G.G., 1978. Manual for tidal currents analysis and prediction. Pacific Marine Science Report 78-6. Institute of Ocean Sciences, Patricia Bay, Sidney, BC. 57 pp.
García Lafuente, J., Almazán, J.L., Fernández, F., Khribeche, A., Hakimi, A., 1990. Sea level in the Strait of Gibraltar: tides. Int. Hydrogr. Rev. LXVII (1), 111–130.
García-Lafuente, J., Vargas, J., Plaza, F., Sarhan, T., Candela, J., Bascheck, B., 2000. Tide at the eastern section of the Strait of Gibraltar. J. Geophys. Res. 105 (C6), 14,197–14,213.
Garcia-Lafuente, J., Delgado, J., Vargas, J.M., Vargas, M., Plaza, F., Sarhan, T., 2002a. Low4 frequency variability of the exchanged flows through the Strait of Gibraltar during CANIGO. Deep Sea Res. Part II 49, 4051–4067.
Garcia-Lafuente, J., Alvarez, E., Vargas, J.M., Ratsimandresey, W., 2002b. Subinertial variability in the flow through the Strait of Gibraltar. J. Geophys. Res. 107 (C10), 32.1–32.9. doi:10.1029/2001JC0011004.
Garrett, C., Bormans, M., Thompson, K., 1990. Is the exchange through the Strait of Gibraltar maximal or submaximal? In: Pratt, L.J. (Ed.), The Physical Oceanography of Sea Straits. Kluwer Academic Publisher, Dordrecht, pp. 271–294.
Lacombe, H., Richez, C., 1982. The regime of the Strait of Gibraltar. In: Nihoul, J.C.J. (Ed.), Hydrodynamics of Semi-Enclosed Seas. Elsevier, Amsterdam, pp. 13–17.
LeBlond, P.H., Mysak, L.A., 1978. Waves in the ocean. Elsevier Oceanographic Series. ISBN: 0-444-41926-8.
Pawlowicz, R., Beardsley, B., Lentz, S., 2002. Classical tidal harmonic analysis including error estimates in Matlab using t tide. Comput. Geosci. 28, 929–937.
Sanchez-Garrido, J.C., García Lafuente, J., Criado Aldeanueva, F., Baquerizo, A., Sannino, G., 2008. Time-spatial variability observed in velocity of propagation of the internal bore in the Strait of Gibraltar. J. Geophys. Res. 113, C07034. doi:10.1029/2007JC004624.
Sánchez-Garrido, J.C., Sannino, G., Liberti, L., García Lafuente, J., Pratt, L., 2011. Numerical modeling of three-dimensional stratified tidal flow over Camarinal Sill, Strait of Gibraltar. J. Geophys. Res. 116, C12026. doi:10.1029/2011JC007093.
Sánchez-Román, A., (2008b), Intercambios a través del Estrecho de Gibraltar y su respuesta a forzamientos de distintas escalas temporales. PhD Thesis, University of Malaga.
Sánchez-Román, A., Criado-Aldeanueva, F., García-Lafuente, J., Garrido, J.S., 2008. Vertical structure of tidal currents over Espartel and Camarinal sills, Strait of Gibraltar. J. Mar. Syst. 74, 120–133. doi:10.1016/j.jmarsys.2007.11.007.
Sánchez-Román, A., Sannino, G., García-Lafuente, J., Carillo, A., Criado-Aldeanueva, F., 2009. Transport estimates at the western section of the Strait of Gibraltar: a combined experimental and numerical modelling study. J. Geophys. Res. 114, C06002. doi:10.1029/2008JC005023.
Sannino, G., Carillo, A., Artale, V., 2007. Three-layer view of transports and hydraulics in the strait of Gibraltar: a three-dimensional model study. J. Geophys. Res. 112. doi:10.1029/2006JC003,717 C03,010.
Sannino, G., Pratt, L., Carillo, A., 2009. Hydraulic criticality of the exchange flow through the Strait of Gibraltar. J. Phys. Oceanogr. 39, 2779–2799. doi:10.1175/2009JPO4075.1.
Soto-Navarro, J., Criado-Aldeanueva, F., García-Lafuente, J., Sánchez-Román, A., 2010. Estimation of the Atlantic inflow through the Strait of Gibraltar from climatological and in situ data. J. Geophys. Res. 115, C10023. doi:10.1029/2010JC006302.
Stommel, H., Farmer, H., 1953. Control of salinity in an estuary by a transition. J. Mar. Res. 12, 13–20.
Tsimplis, M.N., 2000. Vertical structure of tidal currents over the Camarinal sill at the Strait of Gibraltar. J. Geophys. Res. 105, 19709–19728.
Tsimplis, M.N., Bryden, H.L., 2000. Estimation of the transport through the Strait of Gibraltar. Deep Sea Res. Part I 47, 2219–2242.